

Generating Bell states and N -partite W states of long-distance qubits in superconducting waveguide QED

Guo-Qiang Zhang¹, Wei Feng¹, Wei Xiong², Da Xu³, Qi-Ping Su¹, and Chui-Ping Yang^{1,*}

¹*School of Physics, Hangzhou Normal University, Hangzhou, Zhejiang 311121, China*

²*Department of Physics, Wenzhou University, Zhejiang 325035, China*

³*Interdisciplinary Center of Quantum Information, State Key Laboratory of Modern Optical Instrumentation and Zhejiang Province Key Laboratory of Quantum Technology and Device, School of Physics, Zhejiang University, Hangzhou 310027, China*

(Received 9 April 2023; revised 10 September 2023; accepted 15 September 2023; published 5 October 2023)

We show how to generate Bell states and N -partite W states of long-distance superconducting (SC) qubits in a SC waveguide QED system, where SC qubits are coupled to an open microwave transmission line. In the two-qubit case, the Bell state of two long-distance qubits can be a dark state of the system by choosing appropriate system parameters. If one proper microwave pulse drives one of two qubits, the two qubits will evolve from their ground states to a Bell state. Further, we extend this scheme to the multiqubit case. We show that W states of N long-distance qubits can also be generated. Because both the Bell and W states are decoupled from the waveguide (i.e., dark states of the system), they are steady and have very long lifetimes in the ideal case without decoherence of qubits. In contrast to the ideal case, the presence of decoherence of qubits limits the lifetimes of the Bell and W states. Our study provides an alternative scheme for generating Bell states and N -partite W states in SC waveguide QED, which can be used to entangle long-distance nodes in waveguide quantum networks.

DOI: 10.1103/PhysRevApplied.20.044014

I. INTRODUCTION

Due to its fundamental significance for showing quantum nonlocality and diverse applications in quantum technologies, quantum entanglement has attracted substantial interest in the last decades [1,2]. The Bell state refers to the maximally bipartite entangled state [3,4]. Correspondingly, there are two key classes of multipartite entangled states, i.e., Greenberger-Horne-Zeilinger (GHZ) state [5] and W state [6], where the latter is more robust against the loss of excitation [7]. Besides Bell states, GHZ states and W states, the NOON states [8] and Affleck-Kennedy-Lieb-Tasaki (AKLT) states [9] are two useful types of entangled states. Compared to the Bell state, the W state is more favorable in quantum information processing, because it entangles more qubits. To date, Bell states, GHZ states, and W states have been widely studied in, e.g., cavity quantum electrodynamical (QED) systems [10–12], cavity-magnon systems [13,14], superconducting (SC) circuit systems [15–24], and cold neutral atoms [25], where the entangled qubits are short distance. However, in practical applications, it is vital to entangle distant nodes in a quantum network [26–36]. Therefore, generating Bell states, GHZ

states, and W states of long-distance qubits is urgent and necessary [37–41].

The waveguide QED provides an excellent platform for generating long-distance entanglement [42–48], where distant atoms, both natural and artificial, interact with the continuous traveling modes in a one-dimensional (1D) waveguide [49,50]. Experimentally, the waveguide QED has been implemented in quantum dots coupled to a metallic nanowire [51], SC qubits coupled to an open microwave transmission line [52–54], natural atoms coupled to an optical fiber [55–58], nanoparticles coupled to a silica nanofiber [59], and so on. Compared with other waveguide QED systems, the SC waveguide QED system has its unique merits, such as the achievable strong coupling (even ultrastrong coupling) of SC qubit to the open transmission line, the small dissipation of SC qubit, good scalability, and easy controllability [49,50]. Based on SC waveguide QED systems, many exotic phenomena have been explored, such as resonance fluorescence [52], giant SC atoms [60–62], collective Lamb shifts [63], and three-state dressed states [64]. Here, the giant SC atom means that an artificial SC atom is coupled to a SC waveguide at several points, where the dipole approximation is invalid because the distance between different points is comparable to (or larger than) the wavelengths of traveling microwave modes in the waveguide. In optical waveguide

*yangcp@hznu.edu.cn

QED systems, the Bell [65,66] and four-partite W states [67] can be prepared with the assistance of photon counting detection or homodyne detection. Very recently, Ref. [68] has proposed to generate the Bell state with giant SC atoms in a SC waveguide.

In this paper, we propose a scheme for generating the Bell and N -partite W states with long-distance SC qubits in a SC waveguide without need of any measurements. First, we consider two identical SC transmon qubits, Q_1 and Q_2 , coupled to a 1D SC transmission line [see Fig. 1(a)]. Under the Born-Markovian approximation, the considered SC waveguide QED system can be described by a Lindblad master equation [69]. With proper system parameters, we find that the Bell state of Q_1 and Q_2 is exactly a dark state of the waveguide QED system. By driving the qubit Q_1 with a proper microwave pulse, the two-qubit ground state will evolve into a dark state (i.e., the Bell state). Further, the proposed scheme can be easily extended to the multiqubit case. In a SC waveguide QED system with N ($N \geq 3$) long-distance transmon qubits [see Fig. 1(b)], the N -partite W state can also be a dark state of the system by properly choosing the coupling strength of each qubit to the waveguide. Under the drive of an appropriate microwave pulse, the N -partite W state of long-distance qubits can also be generated. In the absence of the intrinsic decoherence of qubits, the generated Bell and N -partite W states are steady because they are decoupled from the SC waveguide. However, in realistic experimental conditions, the decoherence from the qubits determines the lifetimes of the Bell and N -partite W states.

Note that our work is different from Ref. [68] in the following two aspect. First, Ref. [68] is for the generation of Bell states, while our study discusses how to prepare not only Bell states but also N -partite W states. Second, our scheme is based on transmon qubits instead of giant SC atoms used in Ref. [68]. As compared with giant SC atoms, transmon qubits are commonly used and easily fabricated in SC-circuit experiments [50,61]. Because no measurement is required and the initial state is the ground state of the waveguide QED system, our scheme can be easily performed in experiments. The generated Bell and N -partite W states in waveguide QED have potential applications in constructing waveguide quantum networks [65–68].

The paper is organized as follows. In Sec. II, we derive the effective non-Hermitian Hamiltonian of the SC waveguide QED system from the Lindblad master equation. Using the obtained non-Hermitian Hamiltonian, we analyze the eigenvectors and eigenvalues of the waveguide QED system. In Sec. III, we present the scheme for generating Bell states of two long-distance qubits and explain the related physical mechanism using the system eigenvectors. In Sec. IV, we extend the scheme to the multiqubit case and show how to prepare W states of N long-distance qubits. Our discussions and conclusions are given in Sec. V. In addition, three appendices are included. In Appendix A, we derive the master equation of the waveguide QED system with transmon qubits. In Appendix B, we give the parameters used in numerical simulations. In Appendix C, we discuss the effects of the position deviations and the higher levels of transmon qubits on our scheme.

II. MODEL

As illustrated in Fig. 1, N (≥ 2) identical transmon qubits, Q_j located at x_j ($j = 1, 2, \dots, N$), are coupled to a 1D SC transmission line. When Q_1 is driven by a microwave pulse with Rabi frequency Ω_d , the total Hamiltonian of the N transmon qubits is (hereafter assuming $\hbar = 1$)

$$H = \omega_q \sum_{j=1}^N \sigma_j^+ \sigma_j^- + \Theta(t_0 - t) \Omega_d (\sigma_1^+ e^{-i\omega_d t} + \sigma_1^- e^{i\omega_d t}), \quad (1)$$

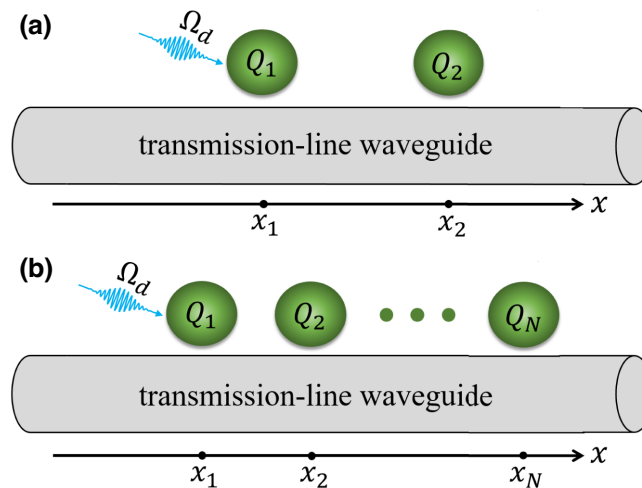


FIG. 1. Schematic diagrams of the considered waveguide QED systems. (a) Two transmon qubits and (b) N (≥ 3) transmon qubits are coupled to a 1D SC transmission line, where the location of the j th qubit Q_j is denoted as x_j . To generate the Bell and N -partite W states, one microwave pulse with Rabi frequency Ω_d drives the qubit Q_1 .

where ω_q is the $|0_j\rangle \leftrightarrow |1_j\rangle$ transition frequency of Q_j with the ground state $|0_j\rangle$ and the excited state $|1_j\rangle$, $\sigma_j^+ = |1_j\rangle\langle 0_j|$ and $\sigma_j^- = |0_j\rangle\langle 1_j|$ are the ladder operators of Q_j , t_0 is the duration of the drive pulse, ω_d is the frequency of the drive pulse, and $\Theta(t_0 - t)$ is the Heaviside function.

By taking trace over the degrees of freedom of the waveguide (i.e., the SC transmission line) at zero temperature, we find that the density operator ρ of N qubits

satisfies the following Born-Markovian master equation (see Appendix A) [69]:

$$\begin{aligned} \frac{\partial \rho}{\partial t} = & -i[H, \rho] + \sum_{j=1}^N \sum_{m=1}^N \frac{\kappa_{jm}}{2} \mathcal{D}[\sigma_j^-, \sigma_m^+] \rho \\ & + \frac{\gamma}{2} \sum_{j=1}^N \mathcal{D}[\sigma_j^-, \sigma_j^+] \rho + \frac{\gamma_\varphi}{2} \sum_{j=1}^N (\sigma_j^z \rho \sigma_j^z - \rho), \quad (2) \end{aligned}$$

with the Lindblad superoperator

$$\mathcal{D}[\sigma_j^-, \sigma_m^+] \rho = 2\sigma_j^- \rho \sigma_m^+ - \sigma_m^+ \sigma_j^- \rho - \rho \sigma_m^+ \sigma_j^-. \quad (3)$$

Note that Eq. (2) is only valid when the location of Q_j is given by $x_j = \pm l\pi/k$ ($l = 0, 1, 2, \dots$), where $k = \omega_q/v$ is the wave vector, and v is the speed of the microwave at frequency ω_q in the waveguide. Here the second term in Eq. (2) presents both the cooperative dissipations and the local dissipations of N qubits caused by the waveguide, where $\kappa_{jm} = 2c_j c_m \kappa$ is the cooperative decay rate of Q_j and Q_m for $j \neq m$ (local decay rate of Q_j for $j = m$), $\kappa = 2\pi g^2 \omega_q$ is the collective decay rate of N qubits, $c_j = (g_j/g)e^{-ikx_j}$ characterizes the relative coupling strength of Q_j to the waveguide, and g (g_j) is the coupling strength between N qubits (Q_j) and the waveguide. In addition, the two terms in the second line of Eq. (2) denote the intrinsic decoherence of N qubits, where γ (γ_φ) is the energy relaxation rate (pure dephasing rate) of the individual qubit, and $\sigma_j^z = |1_j\rangle\langle 1_j| - |0_j\rangle\langle 0_j|$ is the Pauli operator related to Q_j .

In the absence of both the drive pulse and the intrinsic decoherence of N qubits (corresponding to the case with $\Omega_d = \gamma = \gamma_\varphi = 0$), the master equation in Eq. (2) can be rewritten as [70–72]

$$\dot{\rho} = -i(H_{\text{eff}}\rho - \rho H_{\text{eff}}^\dagger) + \sum_{jm} \kappa_{jm} \sigma_j^- \rho \sigma_m^+, \quad (4)$$

where H_{eff} is the effective non-Hermitian Hamiltonian of the waveguide QED system given by

$$\begin{aligned} H_{\text{eff}} = & \sum_{j=1}^N \left(\omega_q - i \frac{\kappa_{jj}}{2} \right) \sigma_j^+ \sigma_j^- \\ & - i \sum_{j=1}^N \sum_{m=j+1}^N \frac{\kappa_{jm}}{2} (\sigma_j^+ \sigma_m^- + \sigma_j^- \sigma_m^+). \quad (5) \end{aligned}$$

For simplicity and clarity, we have ignored the intrinsic decoherence of N qubits in deriving the above effective Hamiltonian. Due to $\gamma, \gamma_\varphi \ll \kappa_{jm}$, it is enough to explain the related physical mechanism of preparing Bell states and W states via using the eigenvectors of H_{eff} (cf. Secs. III and IV). In the effective Hamiltonian H_{eff} , the diagonal non-Hermitian term $-i(\kappa_{jj}/2)\sigma_j^+ \sigma_j^-$ denotes the local

dissipation of the qubit Q_j , while the off-diagonal term $-i(\kappa_{jm}/2)(\sigma_j^+ \sigma_m^- + \sigma_j^- \sigma_m^+)$ presents the dissipative coupling between the qubits Q_j and Q_m [73,74]. By solving $H_{\text{eff}}|\varphi\rangle = E|\varphi\rangle$ in the one-excited subspace, we can obtain the N eigenvectors $\{|\varphi_1\rangle, |\varphi_2\rangle, \dots, |\varphi_N\rangle\}$ of H_{eff} ,

$$\begin{aligned} |\varphi_n\rangle &= c_{n+1}|\phi_1\rangle - c_1|\phi_{n+1}\rangle, \quad n = 1, 2, \dots, N-1, \\ |\varphi_N\rangle &= \sum_{j=1}^N c_j|\phi_j\rangle, \end{aligned} \quad (6)$$

with $|\phi_j\rangle = |0_1 0_2 \dots 0_{j-1} 1_j 0_{j+1} \dots 0_N\rangle$, and the corresponding eigenvalues $E_1 = E_2 = \dots = E_{N-1} = \omega_q$ and $E_N = \omega_q - i \sum_{j=1}^N \kappa_{jj}/2$. Note that the higher-excited subspace is barely involved in preparing the Bell and N -partite W states. Thus, the numerical results related to generating the Bell and W states, which are obtained by numerically solving the master Eq. (2) in the whole Hilbert space, can be well explained by using the eigenvectors (6) in the one-excited subspace (cf. Secs. III and IV). This demonstrates the reasonability of the assumption of the one-excited subspace. From $\text{Im}[E_n] = 0$ ($n = 1, 2, \dots, N-1$) and $\text{Im}[E_N] \neq 0$, the decay rate of the eigenvector $|\varphi_n\rangle$ is zero while the decay rate of the eigenvector $|\varphi_N\rangle$ is nonzero. This indicates that the eigenvectors $\{|\varphi_1\rangle, |\varphi_2\rangle, \dots, |\varphi_{N-1}\rangle\}$ are dark states of the waveguide QED system, and $|\varphi_N\rangle$ is a bright state. The dark state $|\varphi_n\rangle$ is a steady state of the waveguide QED system due to $\partial\rho/\partial t = 0$ with $\rho = |\varphi_n\rangle\langle\varphi_n|$ [75–77]. In contrast, owing to $\partial\rho/\partial t \neq 0$ with $\rho = |\varphi_N\rangle\langle\varphi_N|$, the bright state $|\varphi_N\rangle$ is a nonequilibrium state. In the present work, we use dark states to prepare Bell states and N -partite W states in SC waveguide QED. In addition to preparing entangled states, the dark states also have other potential applications in quantum information processing, including protecting quantum systems from dissipations [75], building gradient memories to store quantum information [76], realizing quantum information protocols in open quantum systems [77], etc.

III. GENERATION OF BELL STATES

In order to generate the Bell states

$$|\Psi_\pm\rangle = \frac{1}{\sqrt{2}}(|10\rangle \pm |01\rangle), \quad (7)$$

we consider a driven waveguide QED system with two transmon qubits, as schematically shown in Fig. 1(a). In the one-excited subspace, the considered waveguide QED system has two orthonormal eigenvectors, the dark state

$|D\rangle$ and the bright state $|B\rangle$ [cf. Eq. (6)],

$$\begin{aligned} |D\rangle &= \frac{1}{\sqrt{c_1^2 + c_2^2}} (c_2|10\rangle - c_1|01\rangle), \\ |B\rangle &= \frac{1}{\sqrt{c_1^2 + c_2^2}} (c_1|10\rangle + c_2|01\rangle). \end{aligned} \quad (8)$$

For $c_1 = -c_2$ ($c_1 = c_2$), $|D\rangle = |\Psi_+\rangle$ and $|B\rangle = |\Psi_-\rangle$ ($|D\rangle = |\Psi_-\rangle$ and $|B\rangle = |\Psi_+\rangle$).

For clarity, we first show the numerical results related to preparing the target state $|\Psi_+\rangle$ in the absence of the intrinsic decoherence of the two qubits (i.e., $\gamma = \gamma_\varphi = 0$). By numerically solving the master equation in Eq. (2) with $c_1 = -c_2$ [78,79], we plot the time evolution of the fidelity $\mathcal{F}_2 = \text{Tr}(\rho|\Psi_+\rangle\langle\Psi_+|)$ in Fig. 2. As shown in Fig. 2(a), under the drive of the microwave pulse on Q_1 , the fidelity \mathcal{F}_2 evolves from 0 to its maximum value $\mathcal{F}_2^{(\max)} = 0.804$ at $t_{\max} = 0.042 \mu\text{s}$ (indicated by the green dot), where we assume that the duration of the microwave pulse is infinite, i.e., $t_0 = +\infty$. This evolution process can be explained using the eigenvectors of the waveguide QED system in Eq. (8). At the initial time $t = 0$, the system of two qubits is

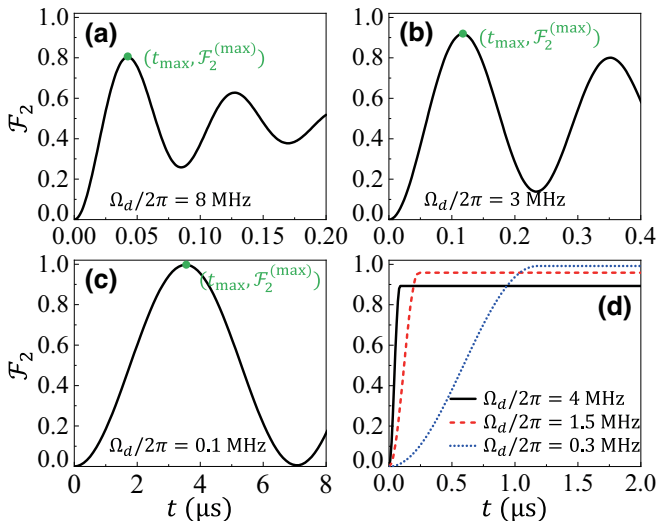


FIG. 2. Time evolution of the fidelity \mathcal{F}_2 of the Bell state $|\Psi_+\rangle$ in the absence of the intrinsic decoherence of the two qubits (i.e., $\gamma = \gamma_\varphi = 0$). (a)–(c) Time evolution of the fidelity \mathcal{F}_2 for different shapes of the drive pulse, where the duration of the drive pulse is $t_0 = +\infty$, while the Rabi frequency is (a) $\Omega_d/2\pi = 8 \text{ MHz}$, (b) $\Omega_d/2\pi = 3 \text{ MHz}$, and (c) $\Omega_d/2\pi = 0.1 \text{ MHz}$. In (a)–(c), the green dots denote the maximum value $\mathcal{F}_2^{(\max)}$ of the fidelity \mathcal{F}_2 at $t = t_{\max}$. (d) Time evolution of the fidelity \mathcal{F}_2 for different values of the Rabi frequency Ω_d , where the duration is $t_0 = t_{\max}$. Here $\Omega_d/2\pi = 4 \text{ MHz}$ and $t_0 = 0.087 \mu\text{s}$ for the (black) solid curve, $\Omega_d/2\pi = 1.5 \text{ MHz}$ and $t_0 = 0.235 \mu\text{s}$ for the (red) dashed curve, and $\Omega_d/2\pi = 0.3 \text{ MHz}$ and $t_0 = 1.176 \mu\text{s}$ for the (blue) dotted curve. Other parameters are chosen as $\omega_q/2\pi = \omega_d/2\pi = 5 \text{ GHz}$, $\kappa_{11}/2\pi = 40 \text{ MHz}$, and $c_1 = -c_2 = 1$.

in the ground state $|00\rangle$ (corresponding to $\mathcal{F}_2 = 0$). Due to the drive pulse on Q_1 , the qubit Q_1 will be excited, and the two-qubit system undergoes the state transformation from the ground state $|00\rangle$ to the one-excited state $|10\rangle$. With the eigenvectors $\{|D\rangle, |B\rangle\}$ (with $|D\rangle = |\Psi_+\rangle$ and $|B\rangle = |\Psi_-\rangle$), the state $|10\rangle$ can be expressed as

$$|10\rangle = \frac{1}{\sqrt{2}}|D\rangle + \frac{1}{\sqrt{2}}|B\rangle, \quad (9)$$

where the component of the bright state $|B\rangle$ will decay to the ground state $|00\rangle$, while the component of the dark state $|D\rangle$ is steady, i.e., the state $|10\rangle$ will evolve to the mixed state of $|00\rangle$ and $|D\rangle$. For the component of $|00\rangle$ in the mixed state, it will be pumped to the one-excited state $|10\rangle$ again, and the process $|00\rangle \rightarrow |10\rangle \rightarrow \{|00\rangle, |D\rangle\}$ is repeated continuously. Ultimately, the waveguide QED system will evolve from the ground state $|00\rangle$ to the dark state $|D\rangle$ (i.e., the Bell state $|\Psi_+\rangle$). It should be noted that the eigenvectors $\{|D\rangle, |B\rangle\}$ are obtained by neglecting the drive pulse. Obviously, if the drive pulse is considered, $|D\rangle$ is not the dark state of the waveguide QED system. As a result, the maximum fidelity is significantly smaller than one (i.e., $\mathcal{F}_2^{(\max)} = 0.804 < 1$) and \mathcal{F}_2 oscillates versus time t [cf. Fig. 2(a)]. To decrease this adverse effect, we can use a weaker drive pulse to achieve a higher fidelity $\mathcal{F}_2^{(\max)}$, while the time t_{\max} for reaching $\mathcal{F}_2^{(\max)}$ is longer [see Figs. 2(b) and 2(c)]. In the weak-drive limit $\Omega_d \rightarrow 0$ with $t_{\max} \rightarrow +\infty$, we can, in principle, generate the Bell state $|\Psi_+\rangle$ with $\mathcal{F}_2^{(\max)} = 1$. For example, $\mathcal{F}_2^{(\max)} = 0.997$ for $\Omega_d/2\pi = 0.1 \text{ MHz}$ with $t_{\max} = 3.518 \mu\text{s}$. Further, by setting $t_0 = t_{\max}$, i.e., the duration of the drive pulse is t_{\max} rather than infinite, the steady Bell state with a fidelity $\mathcal{F}_2^{(\max)}$ can be prepared [see Fig. 2(d)].

Further, we consider the intrinsic decoherence of the two qubits, i.e., $\gamma \neq 0$ and $\gamma_\varphi \neq 0$. In this case, there is a specific drive strength $\Omega_d = \Omega_d^{(\text{opt})}$ (with $\Omega_d^{(\text{opt})}/2\pi = 0.57 \text{ MHz}$) to reach the optimal fidelity $\mathcal{F}_2 = \mathcal{F}_2^{(\text{opt})}$ (with $\mathcal{F}_2^{(\text{opt})} = 0.968$) [cf. Figs. 3(a)–3(c)]. The reason is that if $\Omega_d < \Omega_d^{(\text{opt})}$, the decoherence of Q_1 and Q_2 will dominate the dynamics of the waveguide QED system and spoil the process of generating the target state $|\Psi_+\rangle$. To obtain a long-lived Bell state $|\Psi_+\rangle$, we set the duration of the drive pulse as $t_0 = t_{\text{opt}}$. Now the lifetime of the long-lived Bell state $|\Psi_+\rangle$ is determined by the decoherence times of Q_1 and Q_2 [see Fig. 3(d)]. Obviously, the lifetime of the long-lived Bell state $|\Psi_+\rangle$ is far longer than that of the transient $|\Psi_+\rangle$ [cf. Figs. 3(b) and 3(d)].

With the similar procedures of preparing the Bell state $|\Psi_+\rangle$, we can also generate the other Bell state $|\Psi_-\rangle$ given in Eq. (7) by setting $c_1 = c_2$. In the ideal case without decoherence of Q_1 and Q_2 , the waveguide QED system will evolve from the ground state $|00\rangle$ to the Bell state $|\Psi_-\rangle$ with $\mathcal{F}_{2,-} \rightarrow 1$ in the weak-drive limit $\Omega_d \rightarrow 0$, where

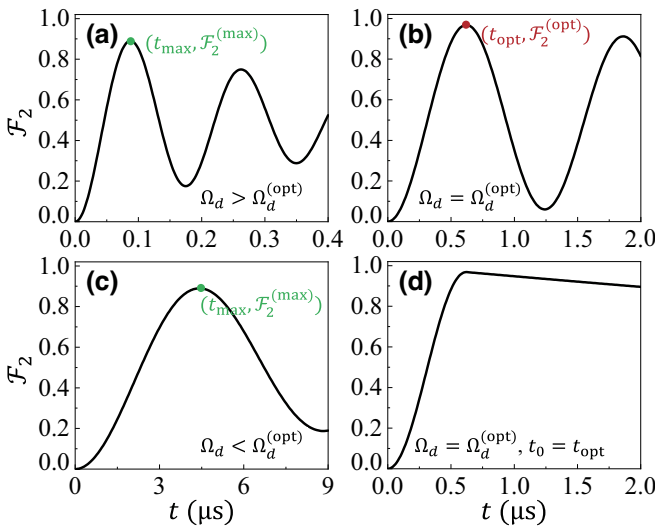


FIG. 3. Time evolution of the fidelity \mathcal{F}_2 of the Bell state $|\Psi_+\rangle$ in the presence of the intrinsic decoherence of the two qubits (e.g., $\gamma^{-1} = 60 \mu\text{s}$ and $\gamma_\varphi^{-1} = 25 \mu\text{s}$). (a)–(c) Time evolution of the fidelity \mathcal{F}_2 for different shapes of the drive pulse, where the duration of the drive pulse is $t_0 = +\infty$, while the Rabi frequency is (a) $\Omega_d = 7.02\Omega_d^{(\text{opt})}$, (b) $\Omega_d = \Omega_d^{(\text{opt})}$, and (c) $\Omega_d = 0.14\Omega_d^{(\text{opt})}$, with $\Omega_d^{(\text{opt})}/2\pi = 0.57 \text{ MHz}$ and $t_{\text{opt}} = 0.623 \mu\text{s}$. In (a),(c), the green dots denote the maximum value $\mathcal{F}_2^{(\max)}$ of the fidelity \mathcal{F}_2 at $t = t_{\max}$, and the red dot denotes the optimal fidelity $\mathcal{F}_2^{(\text{opt})}$ at $t = t_{\text{opt}}$ in (b). (d) Time evolution of the fidelity \mathcal{F}_2 with $\Omega_d = \Omega_d^{(\text{opt})}$ and $t_0 = t_{\text{opt}}$. Other parameters are the same as in Fig. 2.

$\mathcal{F}_{2,-} = \text{Tr } (\rho |\Psi_-\rangle \langle \Psi_-|)$ [see Fig. 4(a)]. Here the generated $|\Psi_-\rangle$ is steady, because it is a dark state of the waveguide QED system. When the decoherence of Q_1 and Q_2 is considered, the long-lived target state $|\Psi_-\rangle$ with $\mathcal{F}_{2,-} = 0.968$ is obtained, where the qubit Q_1 is driven by a microwave pulse with an appropriate shape [see Fig. 4(b)]. Now the lifetime of the generated $|\Psi_-\rangle$ depends on the decoherence times of the two qubits.

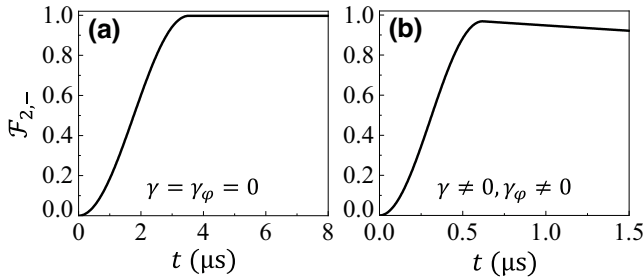


FIG. 4. Time evolution of the fidelity $\mathcal{F}_{2,-}$ of the Bell state $|\Psi_-\rangle$ in (a) the absence of the intrinsic decoherence of Q_1 and Q_2 with $\gamma = \gamma_\varphi = 0$ and (b) the presence of the intrinsic decoherence of Q_1 and Q_2 with $\gamma^{-1} = 60 \mu\text{s}$ and $\gamma_\varphi^{-1} = 25 \mu\text{s}$, where $c_1 = c_2 = 1$. Here $\Omega_d/2\pi = 0.1 \text{ MHz}$ and $t_0 = 3.53 \mu\text{s}$ in (a), while $\Omega_d/2\pi = 0.57 \text{ MHz}$ and $t_0 = 0.623 \mu\text{s}$ in (b). Other parameters are the same as in Fig. 2.

IV. GENERATION OF N -PARTITE W STATES

The scheme proposed in Sec. III can be easily extended to the multiqubit case for preparing the following N -partite W state

$$|W_N\rangle = \frac{1}{\sqrt{N}} \sum_{j=1}^N |\phi_j\rangle, \quad N \geq 3. \quad (10)$$

Here, we consider N identical transmon qubits coupled to a common waveguide, as depicted in Fig. 1(b). In the absence of both the drive field and the intrinsic decoherence of qubits, the effective non-Hermitian Hamiltonian H_{eff} of the waveguide QED system in Eq. (5) has N eigenvectors, i.e., the eigenvectors $\{|\varphi_1\rangle, |\varphi_2\rangle, \dots, |\varphi_{N-1}\rangle\}$ and the eigenvector $|\varphi_N\rangle$ given in Eq. (6), which are the dark states and the bright state of the waveguide QED system, respectively. While these dark states and the bright state are orthogonal (i.e., $\langle \varphi_n | \varphi_N \rangle = 0$), any two of these dark states are not orthogonal (i.e., $\langle \varphi_n | \varphi_m \rangle \neq 0$ with $n \neq m$). Using the Gram-Schmidt orthogonalization, we can obtain a set of orthonormal eigenvectors, $\{|D_1\rangle, |D_2\rangle, \dots, |D_{N-1}\rangle, |B\rangle\}$, where the full expressions for the dark states $\{|D_1\rangle, |D_2\rangle, \dots, |D_{N-1}\rangle\}$ are cumbersome and not shown, and the bright state $|B\rangle$ is given by

$$|B\rangle = \frac{1}{\sqrt{\sum_{j=1}^N c_j^2}} \sum_{j=1}^N c_j |\phi_j\rangle. \quad (11)$$

Now we consider that the N qubits are in the ground state $|0_1 0_2 \dots 0_N\rangle$ at the initial time $t = 0$. By driving the qubit Q_1 , this qubit is excited and the state of the N qubits becomes the one-excited state $|\phi_1\rangle$, which can be expressed as

$$|\phi_1\rangle = \sum_{j=1}^{N-1} p_j |D_j\rangle + p_b |B\rangle, \quad (12)$$

with $p_j = \langle D_j | \phi_1 \rangle$ and $p_b = \langle B | \phi_1 \rangle = c_1 / \sqrt{\sum_{j=1}^N c_j^2}$. For convenience, we define a dark state $|\mathcal{D}\rangle \equiv \sum_{j=1}^{N-1} p_j |D_j\rangle = |\phi_1\rangle - p_b |B\rangle$. In the basis of $|\phi_j\rangle$, the dark state $|\mathcal{D}\rangle$ can be rewritten as

$$|\mathcal{D}\rangle = \sum_{j=1}^N f_j |\phi_j\rangle, \quad (13)$$

where

$$\begin{aligned} f_1 &= 1 - \frac{c_1^2}{\sum_{j=1}^N c_j^2}, \\ f_j &= -\frac{c_1 c_j}{\sum_{j=1}^N c_j^2}, \quad j = 2, 3, \dots, N. \end{aligned} \quad (14)$$

If $f_1 = f_2 = \dots = f_N$, the dark state $|\mathcal{D}\rangle$ can be related to a standard N -partite W state $|W_N\rangle$ given in Eq. (10), i.e., $|\mathcal{D}\rangle \propto |W_N\rangle$. Solving $f_1 = f_2 = \dots = f_N$, we have

$$\begin{aligned} c_1 &= -(N-1)c_2, \\ c_2 &= c_3 = \dots = c_N, \end{aligned} \quad (15)$$

corresponding to $f_1 = f_2 = \dots = f_N = 1/N$. When c_j satisfies Eq. (15), the dark state $|\mathcal{D}\rangle$ in Eq. (13) is reduced to $|\mathcal{D}\rangle = (1/\sqrt{N})|W_N\rangle$. Now Eq. (12) can be rewritten as

$$|\phi_1\rangle = \frac{1}{\sqrt{N}}|W_N\rangle - \frac{c_2}{|c_2|}\sqrt{1 - \frac{1}{N}}|B\rangle, \quad (16)$$

which has the same form as Eq. (9). Here the component of the dark state $|W_N\rangle$ in $|\phi_1\rangle$ is steady, but the component of the bright state $|B\rangle$ will decay to the ground state $|0_10_2\dots0_N\rangle$. Therefore, we can generate the N -partite W state $|W_N\rangle$ by setting $c_1 = -(N-1)c_2$ with $c_2 = c_3 = \dots = c_N$ and driving the qubit Q_1 with an appropriate microwave pulse.

To demonstrate the above analyses, we take the cases of $N = 3, 5$, and 7 as an example. We plot Fig. 5, which shows the maximum value $\mathcal{F}_N^{(\max)}$ of the fidelity $\mathcal{F}_N =$

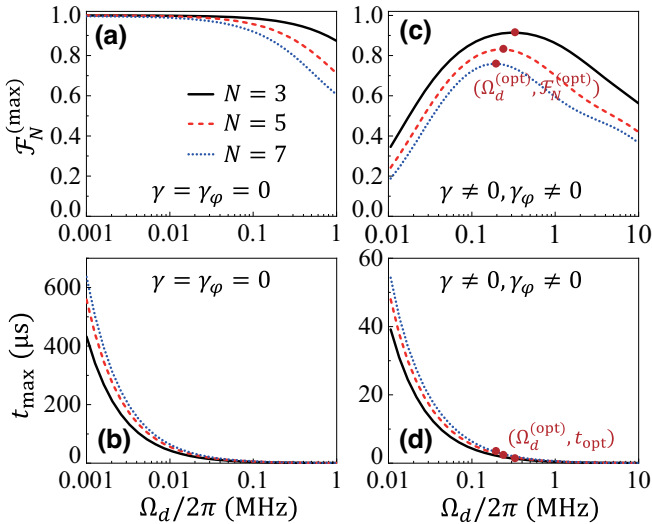


FIG. 5. The maximum fidelity $\mathcal{F}_N^{(\max)}$ of the N -partite W state $|W_N\rangle$ ($N = 3, 5, 7$) versus the Rabi frequency $\Omega_d/2\pi$ in (a) the absence of the intrinsic decoherence of N qubits with $\gamma = \gamma_\varphi = 0$ and (c) the presence of the intrinsic decoherence of N qubits with $\gamma^{-1} = 60 \mu\text{s}$ and $\gamma_\varphi^{-1} = 25 \mu\text{s}$, where $c_1 = N - 1$ and $c_2 = c_3 = \dots = c_N = -1$. For both cases, the corresponding time t_{\max} for reaching $\mathcal{F}_N^{(\max)}$ is shown in (b) and (d), respectively. In (c), the red dots denote that there exists a specific drive strength $\Omega_d = \Omega_d^{(\text{opt})}$ to realize the optimal fidelity $\mathcal{F}_N^{(\text{opt})}$, and the needed time t_{opt} for reaching $\mathcal{F}_N^{(\text{opt})}$ is also marked by the red dots in (d). Other parameters are the same as in Fig. 2.

$\text{Tr}(\rho|W_N\rangle\langle W_N|)$ of the N -partite W state $|W_N\rangle$ and the time t_{\max} for reaching $\mathcal{F}_N^{(\max)}$ as functions of the Rabi frequency $\Omega_d/2\pi$. It should be emphasized that the following discussions and conclusions related to Fig. 5 are valid for any value of N . For $N = 3, 5$, and 7 , both the maximum fidelity $\mathcal{F}_N^{(\max)}$ and the corresponding time t_{\max} versus $\Omega_d/2\pi$ monotonically decrease in the ideal case without the intrinsic decoherence of qubits [see Figs. 5(a) and 5(b)]. In the weak-drive limit $\Omega_d/\kappa_{jj} \rightarrow 0$, one has $\mathcal{F}_N^{(\max)} \rightarrow 1$ but $t_{\max} \rightarrow +\infty$. By choosing the duration $t_0 = t_{\max}$ of the weak-drive pulse (with, e.g., $\Omega_d/2\pi = 0.01$ MHz), a steady W state $|W_N\rangle$ with fidelity $\mathcal{F}_N = \mathcal{F}_N^{(\max)}$ (≥ 0.995) can be prepared [cf. Fig. 6(a)].

When the intrinsic decoherence of qubits is considered, there is a specific value $\Omega_d = \Omega_d^{(\text{opt})}$ of the Rabi frequency for obtaining the optimal fidelity $\mathcal{F}_N = \mathcal{F}_N^{(\text{opt})}$

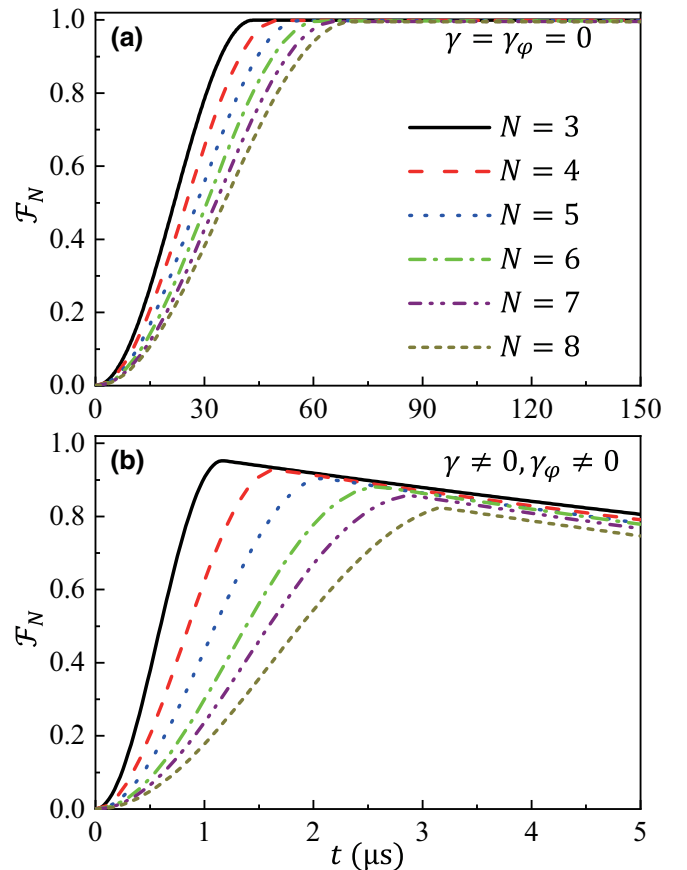


FIG. 6. Time evolution of the fidelity \mathcal{F}_N of the N -partite W state $|W_N\rangle$ ($N = 3, 4, \dots, 8$) in (a) the absence of the intrinsic decoherence of N qubits with $\gamma = \gamma_\varphi = 0$ and (b) the presence of the intrinsic decoherence of N qubits with $\gamma^{-1} = 90 \mu\text{s}$ and $\gamma_\varphi^{-1} = 40 \mu\text{s}$, where $\kappa_{11}/2\pi = 90$ MHz. Here $\Omega_d/2\pi = 0.01$ MHz and $t_0 = t_{\max}$ in (a), while $\Omega_d = \Omega_d^{(\text{opt})}$ and $t_0 = t_{\text{opt}}$ in (b). The values of t_{\max} , $\Omega_d^{(\text{opt})}$ and t_{opt} are given in Appendix B. Other parameters are the same as in Fig. 5.

at time $t = t_{\text{opt}}$ [see Figs. 5(c) and 5(d)]. This characteristic is similar to the case of $N = 2$ [cf. Figs. 3(a)–3(c)]. Under the action of the drive pulse with $\Omega_d = \Omega_d^{(\text{opt})}$ and $t_0 = t_{\text{opt}}$ on Q_1 , the system of N qubits evolves from the ground state $|0_1 0_2 \cdots 0_N\rangle$ to the target state $|W_N\rangle$ with fidelity $\mathcal{F}_N = \mathcal{F}_N^{(\text{opt})}$ [cf. Fig. 6(b)]. Contrary to the ideal case of $\gamma = \gamma_\varphi = 0$, the intrinsic decoherence of qubits limits the lifetime of the generated W state $|W_N\rangle$, and the optimal fidelity $\mathcal{F}_N^{(\text{opt})}$ is smaller than the ideal value 1. Interestingly, we find that after the drive pulses are shut down, the fidelity \mathcal{F}_N versus time decrease at the same rate for different qubit number N . This phenomenon can be explained using an effective non-Hermitian Hamiltonian. Because the generated W state $|W_N\rangle$ is a dark state that decouples from the waveguide, here we consider only the intrinsic decoherence of qubits. Now we can write the effective non-Hermitian Hamiltonian of N qubits as $\mathcal{H}_{\text{eff}} = \sum_{j=1}^N (\omega_q - i\gamma/2) \sigma_j^+ \sigma_j^- - i\gamma_\varphi \sigma_j^z \sigma_j^z / 4$ [70]. Under this effective Hamiltonian, the system of N qubits evolves from the initial state $|\psi(0)\rangle = |W_N\rangle$ to $|\psi(t)\rangle = e^{-i\mathcal{H}_{\text{eff}}t} |\psi(0)\rangle = e^{-i\omega_q t - (\gamma/2 + \gamma_\varphi/4)t} |W_N\rangle$ at time t . Correspondingly, the time evolution of the fidelity is given by $\mathcal{F}_N = |\langle W_N | \psi(t) \rangle|^2 = e^{-(\gamma + \gamma_\varphi/2)t}$, which is independent of the qubit number N .

V. DISCUSSIONS AND CONCLUSIONS

It should be noted that the optimal fidelity $\mathcal{F}_N^{(\text{opt})}$ of the Bell and N -partite W states versus N monotonically decreases when the intrinsic decoherence of qubits is considered [cf. Figs. 6(b) and 7]. This is because the used value of κ_{11} is the same, while the parameter $\kappa_{jj} = \kappa_{11}/(N-1)^2$ ($j \geq 2$) depends on the qubit number N (satisfying $\kappa_{jj} \leq \kappa_{11}$). For given values of κ_{11} , γ , and γ_φ , a smaller N (corresponding to a larger κ_{jj}) makes the conditions $\gamma/\kappa_{jj} \rightarrow 0$ and $\gamma_\varphi/\kappa_{jj} \rightarrow 0$ better satisfied, which results in a larger $\mathcal{F}_N^{(\text{opt})}$. In the limit $\gamma/\kappa_{jj} = \gamma_\varphi/\kappa_{jj} = 0$, $\mathcal{F}_N^{(\text{opt})} \approx 1$ can be obtained [cf. Fig. 6(a)]. Therefore, as shown in Fig. 7, the optimal fidelity $\mathcal{F}_N^{(\text{opt})}$ for a specific N can be improved by increasing the coupling strength of the SC qubit to the waveguide (i.e., larger values of κ_{jj}) [80–82] or using SC qubits with longer decoherence times (i.e., smaller values of γ and γ_φ) [83–86].

Considering the experimentally accessible parameters, we choose $\omega_q/2\pi = 5$ GHz, $\kappa_{jj}/2\pi \leq 90$ MHz, $\gamma^{-1} \leq 90$ μ s, $\gamma_\varphi^{-1} \leq 40$ μ s, and $\Omega_d/2\pi \leq 10$ MHz in the numerical simulations (cf. Figs. 2–7). Note that the specific drive strength $\Omega_d^{(\text{opt})}$ (for reaching the optimal fidelity $\mathcal{F}_N^{(\text{opt})}$) is smaller than 1 MHz, cf. Table II in Appendix B. Experimentally, the strong coupling between the transmon qubit and the waveguide has been demonstrated, where the decay rate $\kappa_{jj}/2\pi = 99.5$ MHz of a transmon qubit, solely induced by a waveguide, is reported [82]. In addition, the typical frequency of a transmon qubit is on the order

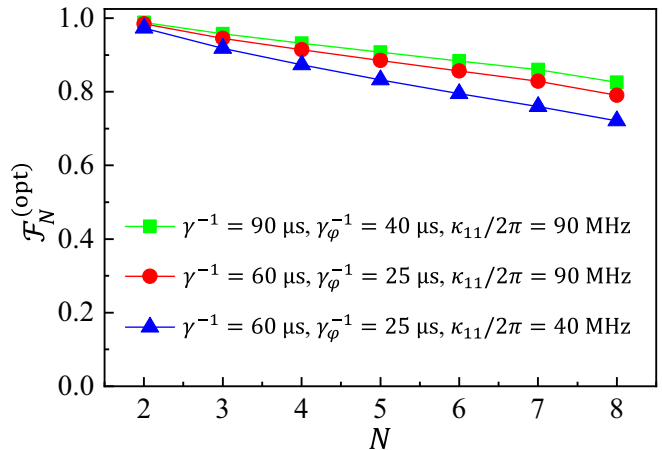


FIG. 7. The optimal fidelity $\mathcal{F}_N^{(\text{opt})}$ of the Bell state $|\Psi_+\rangle$ and N -partite W states $|W_N\rangle$ ($N = 3, 4, \dots, 8$) versus the qubit number N for different energy relaxation rate γ , pure dephasing rate γ_φ and local dissipation rate κ_{11} , where $\Omega_d = \Omega_d^{(\text{opt})}$ and $t_0 = t_{\text{opt}}$. The values of $\Omega_d^{(\text{opt})}$ and t_{opt} can be found in Appendix B. Other parameters are the same as in Fig. 5.

of 1–10 GHz, and the decoherence times γ^{-1} and γ_φ^{-1} of the state-of-the-art transmon qubit are on the order of 10–100 μ s [50, 87–89]. As for the microwave field acting on the qubit, the drive strength of 10 MHz can be easily obtained in experiments [50]. With these experimentally accessible conditions, our scheme can be implemented in the SC waveguide QED system. If transmon qubits are replaced by other types of SC qubits, our scheme is also valid. However, compared with other types of SC qubits, the transmon qubit has its unique advantages, e.g., the simplicity and the flexibility of circuit architectures [90]. Currently, the transmon qubit is the most popular SC qubit. Thus, we use transmon qubits in our scheme.

In our scheme, the generated Bell states $|\Psi_\pm\rangle$ and N -partite W state $|W_N\rangle$ are in the one-excited subspace. In contrast, other two Bell states $|B_\pm\rangle = 1/\sqrt{2}(|11\rangle \pm |00\rangle)$ and N -partite GHZ states involve the higher-excited states $|11\rangle$ and $|1_1 1_2 \cdots 1_N\rangle$, which are not in the one-excited subspace. The higher-excited states $|11\rangle$ and $|1_1 1_2 \cdots 1_N\rangle$ can leak into the one-excited subspace, where there are many stable dark states. This implies that it is difficult to engineer Bell states $|B_\pm\rangle$ and N -partite GHZ states using the present scheme. In addition, it is worth noting that we have ignored the non-Markovian effect in our scheme [cf. Eq. (2) and related discussions], which requires that the distance between any two transmon qubits cannot be too long (i.e., $|x_j - x_m| \ll 10$ m). If the distance between two transmon qubits is on the order of 10 m, the non-Markovian effect in this system should be considered [61]. The impact of non-Markovian effect on our scheme is an interesting topic, which will be investigated in the future.

To summarize, we have presented an alternative scheme for preparing the Bell and N -partite W states of long-distance SC qubits in a SC waveguide. With appropriate system parameters, we find that the Bell state or the N -partite W state is a dark state of the considered SC waveguide QED system. If we drive one of the qubits by a proper microwave pulse, the qubits will evolve from their ground states to the Bell state or the W state. In the ideal case without decoherence of qubits, the prepared Bell and W states are steady since they are decoupled from the waveguide. When the decoherence of SC qubits is considered, the lifetimes of the Bell and W states are on the order of the decoherence times of the qubits. The generated Bell and N -partite W states can be used to entangle long-distance nodes in waveguide QED networks, which is useful in quantum information processing.

ACKNOWLEDGMENTS

This work is supported by the National Natural Science Foundation of China (Grants No. 12205069, No. 12204139, and No. U21A20436), the Key-Area Research and Development Program of GuangDong province (Grant No. 2018B030326001), and the Key Program of the Natural Science Foundation of Anhui (Grant No. KJ2021A1301).

APPENDIX A: THE MASTER EQUATION OF THE WAVEGUIDE QED SYSTEM WITH TRANSMON QUBITS

As shown in Fig. 1, N transmon qubits are coupled to a 1D waveguide (i.e., a SC microwave transmission line) with a continuum of left- and right-propagating microwave modes. For the coupled system, the total Hamiltonian H_{tot} contains three parts:

$$H_{\text{tot}} = H_{\text{sys}} + H_{\text{res}} + H_{\text{int}}. \quad (\text{A1})$$

Here, H_{sys} is the Hamiltonian of N transmon qubits given by

$$H_{\text{sys}} = \sum_{j=1}^N \omega_j \sigma_j^+ \sigma_j^-, \quad (\text{A2})$$

where ω_j is the transition frequency between the ground state $|0_j\rangle$ and the excited state $|1_j\rangle$ of Q_j , and $\sigma_j^- = |0_j\rangle\langle 1_j|$ and $\sigma_j^+ = |1_j\rangle\langle 0_j|$ are the lowering and raising operators of Q_j , respectively. The Hamiltonian H_{res} of the waveguide reads [91]

$$H_{\text{res}} = \int_0^{+\infty} d\nu_k \nu_k [b_L^\dagger(\nu_k)b_L(\nu_k) + b_R^\dagger(\nu_k)b_R(\nu_k)], \quad (\text{A3})$$

where the creation and annihilation operators $b_L(\nu_k)$ and $b_L^\dagger(\nu_k)$ [$b_R(\nu_k)$ and $b_R^\dagger(\nu_k)$] denote the leftward (rightward)

traveling microwave mode at frequency ν_k in the waveguide. Lastly, the electric dipole interactions between the N qubits and the continuum of propagating microwave modes in the waveguide can be expressed as [69]

$$H_{\text{int}} = \sum_{j=1}^N \int_0^{+\infty} d\nu_k g_j \sqrt{\nu_k} [b(\nu_k)\sigma_j^+ + b^\dagger(\nu_k)\sigma_j^-], \quad (\text{A4})$$

with $b(\nu_k) = b_L(\nu_k)e^{-iv_kx_j/v} + b_R(\nu_k)e^{iv_kx_j/v}$, where g_j is the coupling strength of Q_j to the waveguide, x_j is the location of Q_j , and v is the velocity of the microwave in the waveguide.

In the coupled system, the waveguide with continuous propagating modes $b_L(\nu_k)$ and $b_R(\nu_k)$ acts as a common reservoir. At zero temperature, we take trace over the degrees of freedom of the waveguide under both the Born approximation and the Markov approximation. The Born-Markovian master equation for the N qubits can be derived as [69]

$$\begin{aligned} \frac{\partial \rho}{\partial t} &= -i[H_{\text{sys}} + H_{\text{qq}}, \rho] \\ &+ \sum_{j=1}^N \sum_{m=1}^N \frac{\kappa_{jm}}{2} [2\sigma_j^- \rho \sigma_m^+ - \sigma_m^+ \sigma_j^- \rho - \rho \sigma_m^+ \sigma_j^-], \end{aligned} \quad (\text{A5})$$

where ρ is the reduced density operator of the N qubits,

$$H_{\text{qq}} = \sum_{j=1}^N \sum_{m=1}^N \lambda_{jm} \sigma_j^- \sigma_m^+ \quad (\text{A6})$$

describes the interactions among N transmon qubits due to the waveguide, and λ_{jm} (κ_{jm}) is the coherent coupling strength between (cooperative decay rate of) Q_j and Q_m given by

$$\begin{aligned} \lambda_{jm} &= -i\pi g_j g_m (\omega_j e^{ik_j |x_j - x_m|} - \omega_m e^{-ik_m |x_j - x_m|}), \\ \kappa_{jm} &= 2\pi g_j g_m (\omega_j e^{ik_j |x_j - x_m|} + \omega_m e^{-ik_m |x_j - x_m|}). \end{aligned} \quad (\text{A7})$$

Here, $k_j = \omega_j/v$ is the wave vector of the microwave at frequency ω_j . Note that the Markov approximation is reasonable when the distance between any two transmon qubits is on the order of meters [61]. From Eq. (A5), we find that the waveguide has two effects on N qubits. On the one hand, the waveguide mediates the coherent couplings between different qubits and induces the frequency shifts of qubits [corresponding to the Hamiltonian H_{qq} in Eq. (A5)]. On the other hand, the waveguide can cause the cooperative dissipations of different qubits and the local dissipations of qubits [cf. the second term in Eq. (A5)].

When the N qubits are resonant, i.e., $\omega_1 = \omega_2 = \dots = \omega_N = \omega_q$, λ_{jm} and κ_{jm} in Eq. (A7) become

$$\begin{aligned}\lambda_{jm} &= 2\pi g_j g_m \omega_q \sin(k|x_j - x_m|), \\ \kappa_{jm} &= 4\pi g_j g_m \omega_q \cos(k|x_j - x_m|),\end{aligned}\quad (\text{A8})$$

with $k = k_1 = k_2 = \dots = k_N = \omega_q/v$. Obviously, $\lambda_{jm} = \lambda_{mj}$ and $\kappa_{jm} = \kappa_{mj}$. Further, in the case of $kx_j = \pm l\pi$ ($l = 0, 1, 2, \dots$), one has $\lambda_{jm} = 0$ but κ_{jm} can be expressed as

$$\kappa_{jm} = 4\pi g_j g_m \omega_q e^{ik(x_j - x_m)} = 2c_j c_m \kappa, \quad (\text{A9})$$

where we have introduced the collective decay rate $\kappa = 2\pi g^2 \omega_q$ of N qubits, the collective coupling strength g of N qubits to the waveguide, and the relative coupling strength $c_j = (g_j/g)e^{ikx_j}$ of Q_j to the waveguide. Note that c_j is real (i.e., $c_j = c_j^*$) due to $e^{ikx_j} = \pm 1$. Now the coherent coupling between Q_j and Q_m disappears due to $\lambda_{jm} = 0$, and only the cooperative dissipation of Q_j and Q_m exists with $\kappa_{jm} \neq 0$. In this case, Eq. (A5) is reduced to the master equation in Eq. (2) without both the drive pulse and the intrinsic decoherence of N qubits (i.e., $\Omega_d = \gamma = \gamma_\varphi = 0$).

APPENDIX B: THE PARAMETERS USED IN FIGS. 6 AND 7

In Table I, we give the values of t_{\max} , $\Omega_d^{(\text{opt})}$ and t_{opt} used in Fig. 6. In addition, the values of $\Omega_d^{(\text{opt})}$ and t_{opt} used in Fig. 7 are also given in Table II.

APPENDIX C: THE EFFECTS OF THE POSITION DEVIATIONS AND THE HIGHER LEVELS OF TRANSMON QUBITS ON OUR SCHEME

1. The effect of the position deviations of transmon qubits on our scheme

To prepare Bell states and N -partite W states in our scheme, the location of the qubit Q_j is given by $x_j = \pm l\pi/k = \pm l\lambda_0$, where $\lambda_0 = \pi/k = \pi v/\omega_q$. Given that the velocity of the microwave in the waveguide is $v = 10^8$ m/s [69], we find $\lambda_0 = 1$ cm for $\omega_q/2\pi = 5$ GHz. With the experimentally accessible technologies, the position deviation δx of the SC qubits from the ideal position $x_j = \pm l\lambda_0$ can be controlled within 1 μ m (i.e., $\delta x < 1$ μ m). Since

TABLE I. The values of t_{\max} , $\Omega_d^{(\text{opt})}$, and t_{opt} are used in Fig. 6.

Qubit number N	3	4	5	6	7	8
t_{\max} (μ s)	43.3	50.1	55.8	61.4	66.1	70.9
$\Omega_d^{(\text{opt})}/2\pi$ (MHz)	0.370	0.301	0.265	0.233	0.221	0.202
t_{opt} (μ s)	1.165	1.645	2.09	2.606	2.878	3.149

TABLE II. The values of $\Omega_d^{(\text{opt})}$ and t_{opt} are used in Fig. 7, where the second and third lines correspond to the case of $\gamma^{-1} = 60$ μ s, $\gamma_\varphi^{-1} = 25$ μ s, and $\kappa_{11}/2\pi = 40$ MHz, the fourth and fifth lines correspond to the case of $\gamma^{-1} = 60$ μ s, $\gamma_\varphi^{-1} = 25$ μ s, and $\kappa_{11}/2\pi = 90$ MHz, and the sixth and seventh lines correspond to the case of $\gamma^{-1} = 90$ μ s, $\gamma_\varphi^{-1} = 40$ μ s, and $\kappa_{11}/2\pi = 90$ MHz.

Qubit number N	2	3	4	5	6	7	8
$\Omega_d^{(\text{opt})}/2\pi$ (MHz)	0.570	0.310	0.257	0.227	0.205	0.188	0.180
t_{opt} (μ s)	0.623	1.390	1.924	2.431	2.925	3.394	3.530
$\Omega_d^{(\text{opt})}/2\pi$ (MHz)	0.86	0.47	0.37	0.333	0.306	0.279	0.224
t_{opt} (μ s)	0.413	0.917	1.338	1.662	1.974	2.279	2.842
$\Omega_d^{(\text{opt})}/2\pi$ (MHz)	0.69	0.37	0.301	0.265	0.233	0.221	0.202
t_{opt} (μ s)	0.515	1.165	1.645	2.09	2.606	2.878	3.149

the position deviation δx is very small ($\delta x/\lambda_0 < 10^{-4}$), its effect on our scheme is tiny.

To demonstrate the above analyses, we consider an example, i.e., the second qubit Q_2 deviates from the ideal position as an example. In Fig. 8, we plot the optimal fidelity $\mathcal{F}_N^{(\text{opt})}$ of the Bell state $|\Psi_+\rangle$ and N -partite W state $|W_N\rangle$ ($N = 4, 6$) as a function of the position deviation δx of Q_2 , where the position of Q_2 is given by $x_2 = \pi/k + \delta x$. It can be seen that $\mathcal{F}_N^{(\text{opt})}$ versus δx varies slowly around the ideal value $\delta x = 0$. This implies that our scheme is robust to small position deviations of the qubits.

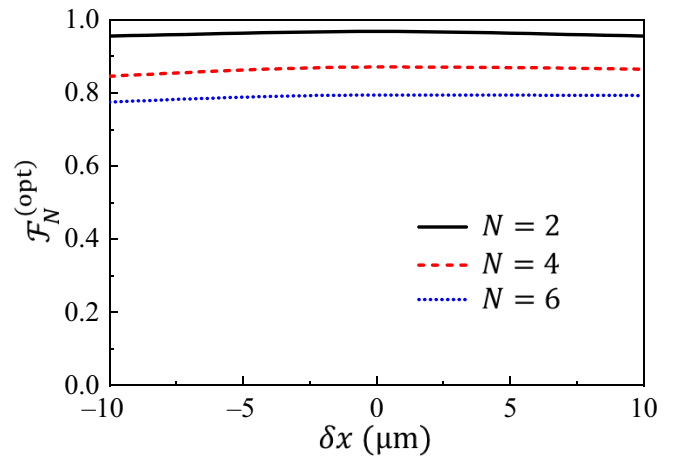


FIG. 8. The optimal fidelity $\mathcal{F}_N^{(\text{opt})}$ of the Bell state $|\Psi_+\rangle$ and N -partite W state $|W_N\rangle$ ($N = 4, 6$) versus the position deviation δx of the second qubit Q_2 , obtained by numerically solving Eq. (A5). In the numerical simulation, the location of Q_2 is set as $x_2 = \pi/k + \delta x$, and other parameters are the same as in Fig. 5(c).

2. The effect of the higher levels of transmon qubits on our scheme

In the main text, we neglect the effect of the higher levels of transmon qubits on our scheme. In the following, we will give some explanations.

When a transmon qutrit is driven by a microwave field with frequency ω_d , the Hamiltonian of the driven qutrit is

$$\begin{aligned} \mathcal{H} = & \omega_{10}|1\rangle\langle 1| + (\omega_{10} + \omega_{21})|2\rangle\langle 2| \\ & + \Omega_d [(|1\rangle\langle 0| + |2\rangle\langle 1|)e^{-i\omega_d t} + \text{H.c.}], \end{aligned} \quad (\text{C1})$$

where $|j\rangle, j = 0, 1, 2$, denotes the lowest three eigenstates of the transmon circuit, ω_{10} (ω_{21}) is the $|0\rangle \leftrightarrow |1\rangle$ ($|1\rangle \leftrightarrow |2\rangle$) transition frequency of the qutrit, and Ω_d is the Rabi frequency of the drive field. For the transmon qutrit, ω_{10} is larger than ω_{21} , i.e., $\omega_{10} > \omega_{21}$ [92]. In the presence of the decoherence of the qutrit, the dynamics of the qutrit is determined by the following Born-Markovian master equation:

$$\begin{aligned} \frac{\partial \rho}{\partial t} = & -i[\mathcal{H}, \rho] + \gamma_{01}\mathcal{L}[|0\rangle\langle 1|]\rho + \gamma_{12}\mathcal{L}[|1\rangle\langle 2|]\rho \\ & + \gamma_{02}\mathcal{L}[|0\rangle\langle 2|]\rho + \gamma_{00}\mathcal{L}[|0\rangle\langle 0|]\rho + \gamma_{11}\mathcal{L}[|1\rangle\langle 1|]\rho \\ & + \gamma_{22}\mathcal{L}[|2\rangle\langle 2|]\rho, \end{aligned} \quad (\text{C2})$$

where $\mathcal{L}[o]\rho = o\rho o^\dagger - o^\dagger o\rho/2 - \rho o^\dagger o/2$, with $o = |j_1\rangle\langle j_2|, j_1 \leq j_2 \in \{0, 1, 2\}$, and the coefficient $\gamma_{j_1 j_2}$ is the corresponding dissipation rate. Note that in Eq. (2), we write the dephasing term as $\sigma_z\rho\sigma_z - \rho$, which is equal to $\mathcal{L}[|1\rangle\langle 1|]\rho + 3\mathcal{L}[|0\rangle\langle 0|]\rho$ if we consider only the ground state $|0\rangle$ and the first-excited state $|1\rangle$.

In our scheme, the drive field is resonant with the $|0\rangle \leftrightarrow |1\rangle$ transition (i.e., $\omega_{10} = \omega_d$) but far detuned from the $|1\rangle \leftrightarrow |2\rangle$ transition, where the detuning $|\omega_{21} - \omega_d|$ between the drive field and the $|1\rangle \leftrightarrow |2\rangle$ transition is equal to the anharmonicity $\eta = \omega_{10} - \omega_{21}$ of the transmon circuit. Experimentally, the typical anharmonicity $\eta/2\pi$ is on the order of 200–300 MHz [92], which is far larger than the optimal drive strength $\Omega_d^{(\text{opt})}/2\pi$ (< 1 MHz; cf. Table II in Appendix B) in our scheme. This indicates that the second-excited state $|2\rangle$ is barely occupied in preparing Bell states and N -partite W states. To enhance this point, we numerically simulate the dynamics of the driven qutrit by numerically solving Eq. (C2). As shown in Fig. 9, even if the qutrit is driven, the second-excited state $|2\rangle$ is nearly not occupied, where the probability $p_2 = \text{Tr}(\rho|2\rangle\langle 2|)$ of the qutrit in the state $|2\rangle$ is always smaller than 0.00005 (i.e., $p_2 < 0.00005$). Thus, it is reasonable to neglect the higher levels of transmon qubits in our scheme.

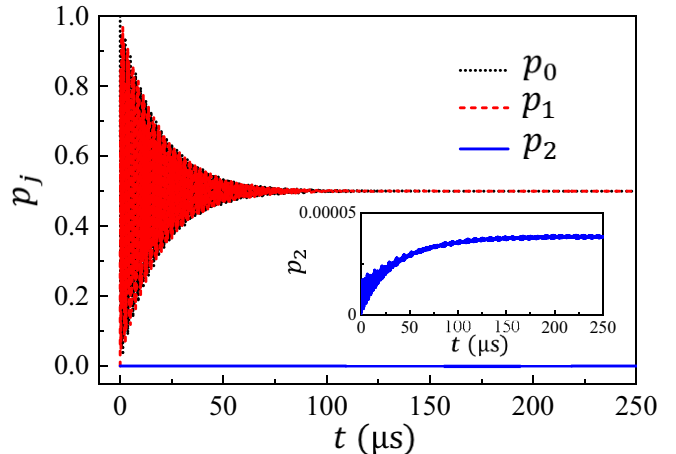


FIG. 9. Time evolution of the probability $p_j = \text{Tr}(\rho|j\rangle\langle j|)$ that the qutrit is in the level $|j\rangle$, obtained by numerically solving Eq. (C2), where $j = 0$ (black dotted curve), $j = 1$ (red dashed curve), and $j = 2$ (blue solid curve). The inset displays the enlarged view of the time evolution of p_2 . In the numerical simulation, we assume that the qutrit is in the ground state $|0\rangle$ at $t = 0$, and other parameters are $\omega_{10}/2\pi = \omega_d/2\pi = 5$ GHz, $\omega_{21}/2\pi = 4.76$ GHz [92], $\Omega_d/2\pi = 1$ MHz, $\gamma_{01}^{-1} = \gamma_{12}^{-1} = 60$ μ s, $\gamma_{02}^{-1} = 150$ μ s, $\gamma_{11}^{-1} = \gamma_{22}^{-1} = 25$ μ s, and $\gamma_{00} = 3\gamma_{11}$.

- [1] R. Horodecki, P. Horodecki, M. Horodecki, and K. Horodecki, Quantum entanglement, *Rev. Mod. Phys.* **81**, 865 (2009).
- [2] L. Aolita, F. D. Melo, and L. Davidovich, Open-system dynamics of entanglement: A key issues review, *Rep. Prog. Phys.* **78**, 042001 (2015).
- [3] P. G. Kwiat, K. Mattle, H. Weinfurter, A. Zeilinger, A. V. Sergienko, and Y. Shih, New high-intensity source of polarization-entangled photon pairs, *Phys. Rev. Lett.* **75**, 4337 (1995).
- [4] L. Quiroga and N. F. Johnson, Entangled Bell and Greenberger-Horne-Zeilinger states of excitons in coupled quantum dots, *Phys. Rev. Lett.* **83**, 2270 (1999).
- [5] D. M. Greenberger, M. A. Horne, A. Shimony, and A. Zeilinger, Bell's theorem without inequalities, *Am. J. Phys.* **58**, 1131 (1990).
- [6] W. Dür, G. Vidal, and J. I. Cirac, Three qubits can be entangled in two inequivalent ways, *Phys. Rev. A* **62**, 062314 (2000).
- [7] N. Brunner, D. Cavalcanti, S. Pironio, V. Scarani, and S. Wehner, Bell nonlocality, *Rev. Mod. Phys.* **86**, 419 (2014).
- [8] B. C. Sanders, Quantum dynamics of the nonlinear rotator and the effects of continual spin measurement, *Phys. Rev. A* **40**, 2417 (1989).
- [9] I. Affleck, T. Kennedy, E. H. Lieb, and H. Tasaki, Rigorous results on valence-bond ground states in antiferromagnets, *Phys. Rev. Lett.* **59**, 799 (1987).
- [10] S. B. Zheng, One-Step synthesis of multiatom Greenberger-Horne-Zeilinger states, *Phys. Rev. Lett.* **87**, 230404 (2001).

- [11] G. P. Guo, C. F. Li, J. Li, and G. C. Guo, Scheme for the preparation of multiparticle entanglement in cavity QED, *Phys. Rev. A* **65**, 042102 (2002).
- [12] Z. J. Deng, M. Feng, and K. L. Gao, Simple scheme for generating an n -qubit W state in cavity QED, *Phys. Rev. A* **73**, 014302 (2006).
- [13] H. Y. Yuan, P. Yan, S. Zheng, Q. Y. He, K. Xia, and M. H. Yung, Steady Bell state generation via magnon-photon coupling, *Phys. Rev. Lett.* **124**, 053602 (2020).
- [14] S. F. Qi and J. Jing, Generation of Bell and Greenberger-Horne-Zeilinger states from a hybrid qubit-photon-magnon system, *Phys. Rev. A* **105**, 022624 (2022).
- [15] M. Ansmann, H. Wang, R. C. Bialczak, M. Hofheinz, E. Lucero, M. Neeley, A. D. O'Connell, D. Sank, M. Weides, J. Wenner, A. N. Cleland, and J. M. Martinis, Violation of Bell's inequality in Josephson phase qubits, *Nature (London)* **461**, 504 (2009).
- [16] M. Neeley, R. C. Bialczak, M. Lenander, E. Lucero, M. Mariantoni, A. D. O'Connell, D. Sank, H. Wang, M. Weides, J. Wenner, Y. Yin, T. Yamamoto, A. N. Cleland, and J. M. Martinis, Generation of three-qubit entangled states using superconducting phase qubits, *Nature (London)* **467**, 570 (2010).
- [17] C. P. Yang, Preparation of n -qubit Greenberger-Horne-Zeilinger entangled states in cavity QED: An approach with tolerance to nonidentical qubit-cavity coupling constants, *Phys. Rev. A* **83**, 062302 (2011).
- [18] C. P. Yang, Q. P. Su, and S. Han, Generation of Greenberger-Horne-Zeilinger entangled states of photons in multiple cavities via a superconducting qutrit or an atom through resonant interaction, *Phys. Rev. A* **86**, 022329 (2012).
- [19] C. P. Yang, Q. P. Su, S. B. Zheng, and S. Han, Generating entanglement between microwave photons and qubits in multiple cavities coupled by a superconducting qutrit, *Phys. Rev. A* **87**, 022320 (2013).
- [20] M. Li, M. Hua, M. Zhang, and F. G. Deng, Entangling two high-Q microwave resonators assisted by a resonator terminated with SQUIDs, *New J. Phys.* **21**, 073025 (2019).
- [21] V. M. Stojanović, Bare-excitation ground state of a spinless-fermion-boson model and W -state engineering in an array of superconducting qubits and resonators, *Phys. Rev. Lett.* **124**, 190504 (2020).
- [22] H. Y. Zhang, Q. P. Su, and C. P. Yang, Efficient scheme for creating a W -type optical entangled coherent state, *Opt. Express* **28**, 35622 (2020).
- [23] J. Peng, J. Zheng, J. Yu, P. Tang, G. A. Barrios, J. Zhong, E. Solano, F. A. Arriagada, and L. Lamata, One-photon solutions to the multiqubit multimode quantum Rabi model for fast W -state Generation, *Phys. Rev. Lett.* **127**, 043604 (2021).
- [24] W. Feng, G. Q. Zhang, Q. P. Su, J. X. Zhang, and C. P. Yang, Generation of Greenberger-Horne-Zeilinger states on two-dimensional superconducting-qubit lattices via parallel multiqubit-gate operations, *Phys. Rev. Appl.* **18**, 064036 (2022).
- [25] V. M. Stojanović, Scalable W -type entanglement resource in neutral-atom arrays with Rydberg-dressed resonant dipole-dipole interaction, *Phys. Rev. A* **103**, 022410 (2021).
- [26] G. Ribordy, J. Brendel, J. D. Gautier, N. Gisin, and H. Zbinden, Long-distance entanglement-based quantum key distribution, *Phys. Rev. A* **63**, 012309 (2000).
- [27] C. Simon and W. T. M. Irvine, Robust long-distance entanglement and a loophole-free bell test with ions and photons, *Phys. Rev. Lett.* **91**, 110405 (2003).
- [28] L. C. Venuti, C. D. E. Boschi, and M. Roncaglia, Long-distance entanglement in spin systems, *Phys. Rev. Lett.* **96**, 247206 (2006).
- [29] B. He, Y. Ren, and J. A. Bergou, Creation of high-quality long-distance entanglement with flexible resources, *Phys. Rev. A* **79**, 052323 (2009).
- [30] J. Zou, S. Zhang, and Y. Tserkovnyak, Bell-state generation for spin qubits via dissipative coupling, *Phys. Rev. B* **106**, L180406 (2022).
- [31] W. K. Mok, J. B. You, L. C. Kwek, and D. Aghamalyan, Microresonators enhancing long-distance dynamical entanglement generation in chiral quantum networks, *Phys. Rev. A* **101**, 053861 (2020).
- [32] X. M. Hu, C. X. Huang, Y. B. Sheng, L. Zhou, B. H. Liu, Y. Guo, C. Zhang, W. B. Xing, Y. F. Huang, C. F. Li, and G. C. Guo, Long-distance entanglement purification for quantum communication, *Phys. Rev. Lett.* **126**, 010503 (2021).
- [33] G. Q. Zhang, W. Feng, W. Xiong, Q. P. Su, and C. P. Yang, Generation of long-lived W states via reservoir engineering in dissipatively coupled systems, *Phys. Rev. A* **107**, 012410 (2023).
- [34] J. B. Brask, I. Rigas, E. S. Polzik, U. L. Andersen, and A. S. Sørensen, Hybrid long-distance entanglement distribution protocol, *Phys. Rev. Lett.* **105**, 160501 (2010).
- [35] L. Trifunovic, F. L. Pedrocchi, and D. Loss, Long-distance entanglement of spin qubits via ferromagnet, *Phys. Rev. X* **3**, 041023 (2013).
- [36] V. Krutyanskiy, M. Galli, V. Krcmarsky, S. Baier, D. A. Fioretto, Y. Pu, A. Mazloom, P. Sekatski, M. Canteri, M. Teller, J. Schupp, J. Bate, M. Meraner, N. Sangouard, B. P. Lanyon, and T. E. Northup, Entanglement of trapped-ion qubits separated by 230 meters, *Phys. Rev. Lett.* **130**, 050803 (2023).
- [37] X. B. Zou, K. Pahlke, and W. Mathis, Generation of an entangled four-photon W state, *Phys. Rev. A* **66**, 044302 (2002).
- [38] M. Eibl, N. Kiesel, M. Bourennane, C. Kurtsiefer, and H. Weinfurter, Experimental realization of a three-qubit entangled W state, *Phys. Rev. Lett.* **92**, 077901 (2004).
- [39] H. Zhou, T. Li, and K. Xia, Parallel and heralded multiqubit entanglement generation for quantum networks, *Phys. Rev. A* **107**, 022428 (2023).
- [40] Y. S. Kim, Y. W. Cho, H. T. Lim, and S. W. Han, Efficient linear optical generation of a multipartite W state via a quantum eraser, *Phys. Rev. A* **101**, 022337 (2020).
- [41] G. L. Jiang, W. Q. Liu, and H. R. Wei, Practically enhanced hyperentanglement concentration for polarization-spatial hyperentangled Bell states with linear optics and common single-photon detectors, *Phys. Rev. Appl.* **19**, 034044 (2023).
- [42] A. Gonzalez-Tudela, D. Martin-Cano, E. Moreno, L. Martin-Moreno, C. Tejedor, and F. J. Garcia-Vidal, Entanglement of two qubits mediated by one-dimensional plasmonic waveguides, *Phys. Rev. Lett.* **106**, 020501 (2011).

- [43] H. Zheng and H. U. Baranger, Persistent quantum beats and long-distance entanglement from waveguide-mediated interactions, *Phys. Rev. Lett.* **110**, 113601 (2013).
- [44] C. Gonzalez-Ballester, A. Gonzalez-Tudela, F. J. Garcia-Vidal, and E. Moreno, Chiral route to spontaneous entanglement generation, *Phys. Rev. B* **92**, 155304 (2015).
- [45] Z. Liao, X. Zeng, S. Y. Zhu, and M. S. Zubairy, Single-photon transport through an atomic chain coupled to a one-dimensional nanophotonic waveguide, *Phys. Rev. A* **92**, 023806 (2015).
- [46] P. Facchi, M. S. Kim, S. Pascazio, F. V. Pepe, D. Pomarico, and T. Tufarelli, Bound states and entanglement generation in waveguide quantum electrodynamics, *Phys. Rev. A* **94**, 043839 (2016).
- [47] I. M. Mirza and J. C. Schotland, Multiqubit entanglement in bidirectional-chiral-waveguide QED, *Phys. Rev. A* **94**, 012302 (2016).
- [48] Z. B. Yang, Y. P. Wang, J. Li, C. M. Hu, and J. Q. You, Entanglement emerges from dissipation-structured quantum self-organization, *J. Magn. Magn. Mater.* **564**, 170139 (2022).
- [49] D. Roy, C. M. Wilson, and O. Firstenberg, Colloquium: Strongly interacting photons in one-dimensional continuum, *Rev. Mod. Phys.* **89**, 021001 (2017).
- [50] X. Gu, A. F. Kockum, A. Miranowicz, Y.-x. Liu, and F. Nori, Microwave photonics with superconducting quantum circuits, *Phys. Rep.* **718**, 1 (2017).
- [51] A. V. Akimov, A. Mukherjee, C. L. Yu, D. E. Chang, A. S. Zibrov, P. R. Hemmer, H. Park, and M. D. Lukin, Generation of single optical plasmons in metallic nanowires coupled to quantum dots, *Nature (London)* **450**, 402 (2007).
- [52] O. Astafiev, A. M. Zagorskin, A. A. Abdumalikov, Y. A. Pashkin, T. Yamamoto, K. Inomata, Y. Nakamura, and J. S. Tsai, Resonance fluorescence of a single artificial atom, *Science* **327**, 840 (2010).
- [53] I. C. Hoi, T. Palomaki, J. Lindkvist, G. Johansson, P. Delsing, and C. M. Wilson, Generation of nonclassical microwave states using an artificial atom in 1d open space, *Phys. Rev. Lett.* **108**, 263601 (2012).
- [54] I. C. Hoi, A. F. Kockum, L. Tornberg, A. Pourkabirian, G. Johansson, P. Delsing, and C. M. Wilson, Probing the quantum vacuum with an artificial atom in front of a mirror, *Nat. Phys.* **11**, 1045 (2015).
- [55] M. Bajcsy, S. Hofferberth, V. Balic, T. Peyronel, M. Hafezi, A. S. Zibrov, V. Vuletic, and M. D. Lukin, Efficient all-optical switching using slow light within a hollow fiber, *Phys. Rev. Lett.* **102**, 203902 (2009).
- [56] A. Goban, K. S. Choi, D. J. Alton, D. Ding, C. Lacroûte, M. Pototschnig, T. Thiele, N. P. Stern, and H. J. Kimble, Demonstration of a state-insensitive, compensated nanofiber trap, *Phys. Rev. Lett.* **109**, 033603 (2012).
- [57] H. L. Sørensen, J. B. Béguin, K. W. Kluge, I. Iakoupov, A. S. Sørensen, J. H. Müller, E. S. Polzik, and J. Appel, Coherent backscattering of light off one-dimensional atomic strings, *Phys. Rev. Lett.* **117**, 133604 (2016).
- [58] N. V. Corzo, B. Gouraud, A. Chandra, A. Goban, A. S. Sheremet, D. V. Kupriyanov, and J. Laurat, Large Bragg reflection from one-dimensional chains of trapped atoms near a nanoscale waveguide, *Phys. Rev. Lett.* **117**, 133603 (2016).
- [59] J. Petersen, J. Volz, and A. Rauschenbeutel, Chiral nanophotonic waveguide interface based on spin-orbit interaction of light, *Science* **346**, 67 (2014).
- [60] A. F. Kockum, G. Johansson, and F. Nori, Decoherence-free interaction between giant atoms in waveguide quantum electrodynamics, *Phys. Rev. Lett.* **120**, 140404 (2018).
- [61] B. Kannan, M. J. Ruckriegel, D. L. Campbell, A. F. Kockum, J. Braumüller, D. K. Kim, M. Kjaergaard, P. Krantz, A. Melville, B. M. Niedzielski, A. Vepsäläinen, R. Winik, J. L. Yoder, F. Nori, T. P. Orlando, S. Gustavsson, and W. D. Oliver, Waveguide quantum electrodynamics with superconducting artificial giant atoms, *Nature (London)* **583**, 775 (2020).
- [62] A. M. Vadiraj, A. Ask, T. G. McConkey, I. Nsanzineza, C. W. S. Chang, A. F. Kockum, and C. M. Wilson, Engineering the level structure of a giant artificial atom in waveguide quantum electrodynamics, *Phys. Rev. A* **103**, 023710 (2021).
- [63] P. Y. Wen, K. T. Lin, A. F. Kockum, B. Suri, H. Ian, J. C. Chen, S. Y. Mao, C. C. Chiu, P. Delsing, F. Nori, G. D. Lin, and I. C. Hoi, Large Collective Lamb shift of two distant superconducting artificial atoms, *Phys. Rev. Lett.* **123**, 233602 (2019).
- [64] K. Koshino, H. Terai, K. Inomata, T. Yamamoto, W. Qiu, Z. Wang, and Y. Nakamura, Observation of the three-state dressed states in circuit quantum electrodynamics, *Phys. Rev. Lett.* **110**, 263601 (2013).
- [65] X. H. H. Zhang and H. U. Baranger, Heralded Bell state of dissipative qubits using classical light in a waveguide, *Phys. Rev. Lett.* **122**, 140502 (2019).
- [66] H. Zhan and H. Tan, Long-time Bell states of waveguide mediated qubits via continuous measurement, *Phys. Rev. A* **105**, 033715 (2022).
- [67] G. Z. Song, M. J. Tao, J. Qiu, and H. R. Wei, Quantum entanglement creation based on quantum scattering in one-dimensional waveguides, *Phys. Rev. A* **106**, 032416 (2022).
- [68] A. C. Santos and R. Bachelard, Generation of maximally entangled long-lived states with giant atoms in a waveguide, *Phys. Rev. Lett.* **130**, 053601 (2023).
- [69] K. Lalumi  re, B. C. Sanders, A. F. van Loo, A. Fedorov, A. Wallraff, and A. Blais, Input-output theory for waveguide QED with an ensemble of inhomogeneous atoms, *Phys. Rev. A* **88**, 043806 (2013).
- [70] F. Minganti, A. Miranowicz, R. W. Chhajlany, and F. Nori, Quantum exceptional points of non-Hermitian Hamiltonians and Liouvillians: The effects of quantum jumps, *Phys. Rev. A* **100**, 062131 (2019).
- [71] G. Q. Zhang, Z. Chen, D. Xu, N. Shammah, M. Liao, T. F. Li, L. Tong, S. Y. Zhu, F. Nori, and J. Q. You, Exceptional point and cross-relaxation effect in a hybrid quantum system, *PRX Quantum* **2**, 020307 (2021).
- [72] W. Chen, M. Abbasi, Y. N. Joglekar, and K. W. Murch, Quantum jumps in the non-Hermitian dynamics of a superconducting qubit, *Phys. Rev. Lett.* **127**, 140504 (2021).
- [73] M. Harder, Y. Yang, B. M. Yao, C. H. Yu, J. W. Rao, Y. S. Gui, R. L. Stamps, and C. M. Hu, Level attraction due to dissipative magnon-photon coupling, *Phys. Rev. Lett.* **121**, 137203 (2018).
- [74] Y. Wang, W. Xiong, Z. Xu, G. Q. Zhang, and J. Q. You, Dissipation-induced nonreciprocal magnon blockade

- in a magnon-based hybrid system, *Sci. China-Phys. Mech. Astron.* **65**, 260314 (2022).
- [75] C. Dong, V. Fiore, M. C. Kuzyk, and H. Wang, Optomechanical dark mode, *Science* **338**, 1609 (2012).
- [76] X. Zhang, C. L. Zou, N. Zhu, F. Marquardt, L. Jiang, and H. X. Tang, Magnon dark modes and gradient memory, *Nat. Commun.* **6**, 8914 (2015).
- [77] M. Zanner, T. Orell, C. M. F. Schneider, R. Albert, S. Oleschko, M. L. Juan, M. Silveri, and G. Kirchmair, Coherent control of a multi-qubit dark state in waveguide quantum electrodynamics, *Nat. Phys.* **18**, 538 (2022).
- [78] J. R. Johansson, P. D. Nation, and F. Nori, QuTiP: An open-source Python framework for the dynamics of open quantum systems, *Comput. Phys. Commun.* **183**, 1760 (2012).
- [79] J. R. Johansson, P. D. Nation, and F. Nori, QuTiP 2: A Python framework for the dynamics of open quantum systems, *Comput. Phys. Commun.* **184**, 1234 (2013).
- [80] I. C. Hoi, C. M. Wilson, G. Johansson, T. Palomaki, B. Peropadre, and P. Delsing, Demonstration of a single-photon router in the microwave regime, *Phys. Rev. Lett.* **107**, 073601 (2011).
- [81] P. Forn-Díaz, J. J. García-Ripoll, B. Peropadre, J. L. Orgiazzi, M. A. Yurtalan, R. Belyansky, C. M. Wilson, and A. Lupascu, Ultrastrong coupling of a single artificial atom to an electromagnetic continuum in the nonperturbative regime, *Nat. Phys.* **13**, 39 (2017).
- [82] M. Mirhosseini, E. Kim, X. Zhang, A. Sipahigil, P. B. Dieterle, A. J. Keller, A. Asenjo-Garcia, D. E. Chang, and O. Painter, Cavity quantum electrodynamics with atom-like mirrors, *Nature (London)* **569**, 692 (2019).
- [83] T. W. Larsen, K. D. Petersson, F. Kuemmeth, T. S. Jespersen, P. Krogstrup, J. Nygård, and C. M. Marcus, Semiconductor-nanowire-based superconducting qubit, *Phys. Rev. Lett.* **115**, 127001 (2015).
- [84] J. Q. You, X. Hu, S. Ashhab, and F. Nori, Low-decoherence flux qubit, *Phys. Rev. B* **75**, 140515(R) (2007).
- [85] N. Earnest, S. Chakram, Y. Lu, N. Irons, R. K. Naik, N. Leung, L. Ocola, D. A. Czaplewski, B. Baker, J. Lawrence, J. Koch, and D. I. Schuster, Realization of a Λ system with metastable states of a capacitively shunted fluxonium, *Phys. Rev. Lett.* **120**, 150504 (2018).
- [86] I. Siddiqi, Engineering high-coherence superconducting qubits, *Nat. Rev. Mater.* **6**, 875 (2021).
- [87] C. Rigetti, J. M. Gambetta, S. Poletto, B. L. T. Plourde, J. M. Chow, A. D. Córcoles, J. A. Smolin, S. T. Merkel, J. R. Rozen, G. A. Keefe, M. B. Rothwell, M. B. Ketchen, and M. Steffen, Superconducting qubit in a waveguide cavity with a coherence time approaching 0.1 ms, *Phys. Rev. B* **86**, 100506 (2012).
- [88] J. B. Chang, M. R. Vissers, A. D. Córcoles, M. Sandberg, J. Gao, D. W. Abraham, J. M. Chow, J. M. Gambetta, M. B. Rothwell, G. A. Keefe, M. Steffen, and D. P. Pappas, Improved superconducting qubit coherence using titanium nitride, *Appl. Phys. Lett.* **103**, 012602 (2013).
- [89] K. X. Wei, I. Lauer, S. Srinivasan, N. Sundaresan, D. T. McClure, D. Toyli, D. C. McKay, J. M. Gambetta, and S. Sheldon, Verifying multipartite entangled Greenberger-Horne-Zeilinger states via multiple quantum coherences, *Phys. Rev. A* **101**, 032343 (2020).
- [90] H. L. Huang, D. Wu, D. Fan, and X. Zhu, Superconducting quantum computing: A review, *Sci. China Inf. Sci.* **63**, 180501 (2020).
- [91] J. T. Shen and S. Fan, Coherent single photon transport in a one-dimensional waveguide coupled with superconducting quantum bits, *Phys. Rev. Lett.* **95**, 213001 (2005).
- [92] D. W. Wang, C. Song, W. Feng, H. Cai, D. Xu, H. Deng, H. Li, D. Zheng, X. Zhu, H. Wang, S. Y. Zhu, and M. O. Scully, Synthesis of antisymmetric spin exchange interaction and chiral spin clusters in superconducting circuits, *Nat. Phys.* **15**, 382 (2019).